Enhancement of photoluminescence from excitons in silicon nanocrystals via coupling to surface plasmon polaritons

Eiji Takeda, Minoru Fujii,[a] Toshihiro Nakamura, Yugo Mochizuki, and Shinji Hayashi
Department of Electrical and Electronic Engineering, Faculty of Engineering, Kobe University, Rokkodai, Nada, Kobe 657-8501, Japan

(Received 27 March 2007; accepted 29 May 2007; published online 17 July 2007)

The enhancement of photoluminescence (PL) is demonstrated from silicon nanocrystals (Si-ncs) by strong coupling of excitons to surface plasmon polaritons (SPPs) supported by a Au thin film. SPPs excited via excitons in Si-ncs were Bragg scattered to photons by one- or two-dimensional gratings, and strong and directional PL was obtained. From the angular dependence of PL spectra, dispersion relations of electromagnetic modes involved in the light emission process were obtained. The overall agreement between experimentally obtained and theoretically calculated dispersion relations confirmed that the strong and directional PL is mediated by SPPs. The PL decay rate of Si-ncs increased by placing a Au thin film on top and the wavelength dependence of the rate enhancement agreed well with that of the calculated SPP excitation rate. This suggests that the observed PL enhancement is due to efficient energy transfer from excitons to SPPs followed by efficient scattering of SPPs to photons, resulting in the enhancement of luminescence quantum efficiency.
 [DOI: 10.1063/1.2753571]

I. INTRODUCTION

Silicon nanocrystals (Si-ncs) show photoluminescence (PL) at room temperature due to the recombination of excitons confined in a zero-dimensional quantum confined system.[1–4] As excitons are confined in a space smaller than the exciton Bohr radius of bulk Si crystals, the overlap of electron and hole wave functions becomes larger in both real and momentum spaces, resulting in the enhancement of the radiative recombination rate.[2,3] However, even for Si-ncs as small as a few nanometers in diameter, the indirect band gap nature of bulk Si crystals is strongly inherited,[5] and thus the spontaneous emission rate is still not large enough compared to that of the direct band gap semiconductor and the luminescence quantum efficiency is rather low.[2,3] Therefore, the enhancement of luminescence efficiency of Si-ncs is in high demand for its application to optoelectric devices.

One of the approaches to enhance luminescence efficiency of Si-ncs is to realize the coupling of electronic excitation of Si-ncs to surface plasmon polaritons (SPPs) supported by metal nanostructures. For example, by placing a nanoporous Au layer near Si-ncs, enhancement of PL from Si-ncs was demonstrated.[6] The SPP resonance energy of metal nanostructures can be tuned in a wide wavelength range by controlling the size and shape. In fact, the enhancement of PL from Si-ncs at specific wavelength ranges has been shown by placing an Ag island array with different sizes and pitches.[7] Further, polarization-selective enhancement of PL is realized by using an anisotropic metal structure.[8]

PL enhancement is also possible by using a flat thin metal film if SPPs are scattered properly and converted to photons efficiently. In previous work, it was demonstrated that strong directional PL from Si-ncs caused by the coupling of electronic excitation of Si-ncs and SPPs supported by a metal thin film and the scattering of the SPPs by a one-dimensional (1D) organic grating. One advantage of using a flat metal film and a grating to convert electronic excitation to photons via SPPs is that dispersion relations are obtained from angle-resolved PL spectra and by analyzing the relation, the origin (mode) of PL peaks can be identified unambiguously.[9] However, in the previous work using a 1D grating, the degree of the enhancement was limited. This is because only SPPs having the momentum to the direction parallel to the grating vector can be Bragg scattered and converted to photons and others are lost to heat.[10] This problem is overcome by using a two-dimensional (2D) grating, which has two orthogonal grating vectors and can scatter SPPs propagating in all in-plane directions to photons.[11]

In this work, we study PL from Si-ncs for the samples consisting of SiO_2 films containing Si-ncs, a flat thin Au film, and a 1D or 2D organic grating. Dispersion relations from angle-resolved PL spectra are obtained, and from the dispersion relations, the modes contributing to the PL enhancement are discussed. The coupling of electronic excitation of Si-ncs to SPPs results in the enhancement of the PL decay rate. From the comparison between experimentally obtained wavelength dependence of the PL decay rate enhancement and calculated power dissipation to SPPs and other modes, the mechanisms of the rate enhancement and also the intensity enhancement are discussed.

II. EXPERIMENTAL PROCEDURE

SiO_2 films containing Si-ncs (Si-nc:SiO_2 films) were prepared by a cosputtering method.[12–14] Si and SiO_2 were simultaneously sputter deposited on a SiO_2 substrate, and the deposited films (150 nm in thickness) were annealed in a nitrogen gas atmosphere for 30 min at 1250 °C. Si-ncs were grown in the films during the annealing. After the annealing,

[a]Electronic mail: fujii@eedept.kobe-u.ac.jp

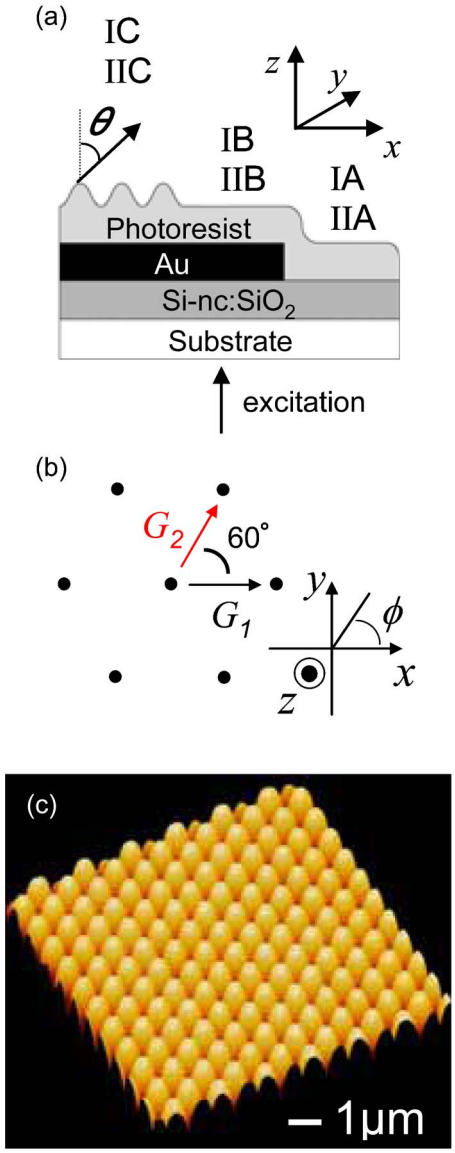

FIG. 1. (Color online) (a) Schematic illustration of sample structure, (b) definition of grating vectors and coordinates, and (c) AFM image of the surface of the sample with a 2D grating.

a Au film 50 nm in thickness was deposited. The corrugated surface was obtained by exposing a photoresist (TDMR-AR80 HP, Tokyo Ohka Kogyo) film spin coated on a Au film to an interference pattern produced with a 325 nm line of a He-Cd laser. Subsequent exposure after the rotation of the sample by 60° about the surface normal resulted in a hexagonal 2D corrugation. The schematic illustration of the sample structure, the definition of the grating vectors ($\mathbf{G}_1$ and $\mathbf{G}_2$) and coordinates, and an atomic force microscope (AFM) image of the surface of the sample with a 2D grating are shown in Figs. 1(a)–1(c), respectively. As shown in Fig. 1(a), we refer the sample with a flat photoresist layer to sample IIA, that with flat photoresist and Au layers to sample IIB, and that with 2D grating on top of the Au layer to sample IIC. We also prepared similar series of samples with a 1D grating. These samples are referred to samples IA, IB, and IC.

In order to measure angular dependence of PL spectra

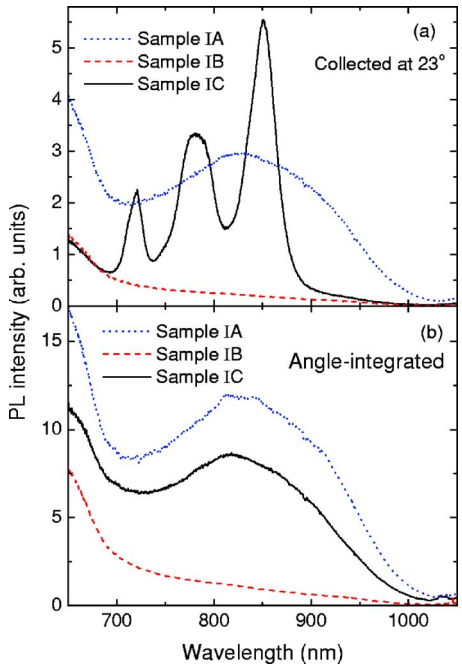

FIG. 2. (Color online) (a) PL spectra collected at θ=23° for the sample with a flat photoresist layer (sample IA) (dotted line), that with flat photoresist and Au layers (sample IB) (dashed line), and that with 1D grating on top of a Au layer (sample IC) (solid line). (b) Angle-integrated PL spectra for samples IA (dotted line), IB (dashed line), and IC (solid line).

from the corrugated surface, samples were mounted on a rotating stage with the grating vector $\mathbf{G}_1$ parallel to the incident plane, and illuminated through the transparent fused-quartz substrate. The excitation source was a 488 nm line of an Ar ion laser. The excitation light was incident normal to the surface, whereas the collection angle θ was changed from 0° (normal to the surface) to 60°. PL was collected from the corrugated side through an aperture approximately 1 mm in diameter, which limits the angular acceptance to about 1°. PL spectra were measured by using a single grating monochromator with a liquid nitrogen cooled Si charge coupled device. The spectral response of the detection system was calibrated with the aid of a reference spectrum of a standard tungsten lamp.

For time-resolved PL measurements, the samples were excited by a 488 nm line of an optical parametric oscillator pumped by the third harmonic of a neodium:yttrium–aluminum–garnet laser (pulse energy 0.5 mJ/cm^2, pulse width 5 ns and repetition frequency 20 Hz) through a transparent fused-quartz substrate. The signals were detected either from the grating side or from the substrate side by a near infrared photomultiplier tube (R5509-72, Hamamatsu Photonics) and a multichannel scaler (SR430, Stanford Research Systems). The time resolution of the system was 5.12 μs. The detection wavelengths were changed from 800 to 1000 nm.

III. RESULTS AND DISCUSSION

A. PL spectra and dispersion relations

Figure 2(a) shows the PL spectra for samples IA, IB, and IC collected at θ=23°. The PL band covering the 700–1000

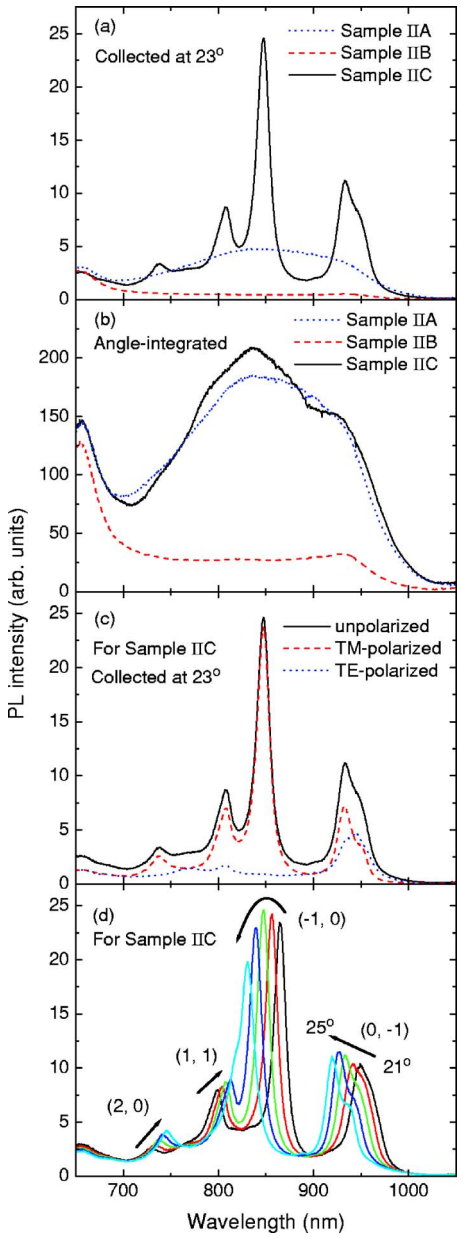

FIG. 3. (Color online) (a) PL spectra collected at $\theta=23°$ for the sample with a flat photoresist layer (sample IIA) (dotted line), that with flat photoresist and Au layers (sample IIB) (dashed line), and that with 2D grating on top of a Au layer (sample IIC) (solid line). (b) Angle-integrated PL spectra for samples IIA (dotted line), IIB (dashed line), and IIC (solid line). (c) Polarization-resolved PL spectra of sample IIC at $\theta=23°$. Solid, dashed, and dotted lines represent unpolarized, TM polarized and TE polarized emission, respectively. (d) Angular dependence of PL spectra of sample IIC. The detection angle θ is changed from 21° to 25°. The numbers (m,n) represent the orders of the scattering processes of SPP modes associated with the interface between Au and Si-nc:SiO_2 layers.

nm range arises from Si-ncs, whereas that below 700 nm from the photoresist. In the following, we will pay attention only to the PL from Si-ncs. In Fig. 2(a), in the presence of the grating, the shape of the PL spectrum is strongly modified and several peaks are observed. At the wavelength of the highest PL intensity of sample IC, the intensity is enhanced by a factor of 2 compared to that of sample IA and by a factor of 30 compared to that of sample IB. To compare the integrated PL intensities among the samples, the spectra are measured in the polar angle range from 10° to 60° in 1° intervals and are summed together. The results are shown in Fig. 2(b). For a 1D grating, the integrated PL intensity of sample IC is larger than that of sample IB but is smaller than that of sample IA.

Figure 3(a) shows the PL spectra for samples IIA, IIB, and IIC collected at $\theta=23°$. Compared to the sample with the 1D grating (sample IC), the peaks are sharper and the number of the peaks increases. Further, the enhancement of the intensity is more pronounced, i.e., the enhancement factors are 5.2 compared to that of sample IIA and 57 compared to that of sample IIB. As can be seen in Fig. 3(b), the integrated PL intensity for sample IIC is slightly larger than that for sample IIA. This is due to the scattering of SPPs propagating in all in-plane direction by the 2D grating.[15]

Figure 3(c) shows polarization-resolved PL spectra for sample IIC at $\theta=23°$. Solid, dashed and dotted lines represent unpolarized, transverse magnetic (TM) polarized, and transverse electric (TE) polarized emissions, respectively. TE and TM polarization are defined as their electric field being perpendicular and parallel to the $x-z$ plane, respectively. The peaks at 740 and 850 nm are TM polarized, whereas those at 810 and 930 nm have both the TM and TE polarization components. Figure 3(d) shows angular dependence of PL spectra for sample IIC. We can see the shift of the peaks by increasing the collection angle. The shift is due to Bragg scattering of SPP or waveguide modes. From the angular dependence of PL peak wavelengths, the dispersion relations are obtained. The experimentally obtained dispersion relations are shown in Fig. 4 by open and closed circles, and squares. To facilitate the assignment of the data, the same experimental data are displayed in Figs. 4(a)–4(d).

In order to assign the modes, we calculate the dispersion relations by the formalism developed by Chance *et al.*[16] by assuming a five-layer system consisting of air/photoresist/Au/Si-nc:SiO_2/SiO_2.[9,17,18] In the calculation, an emitter is regarded as an oscillating electric dipole and the power dissipated from an isotropic dipole positioned at the center of an optically active Si-nc:SiO_2 layer is calculated as a function of an in-plane wave vector. For the calculation, the refractive indices of Au, Si, and SiO_2 are taken from the literature[19–21] and that of the Si-nc:SiO_2 layer is estimated from the Bruggeman effective medium theory.[22] The refractive index of the photoresist layer is obtained by a noncontact thin film metrology system (FilmTek 1000, Scientific Computing International). The wavelength dispersion of the refractive indices of Au, Si, SiO_2 and the photoresist are taken into account. In the presence of a grating the wave vector of SPP or waveguide modes is augmented or reduced, and the modes can couple to photons. For a 2D grating, the coupling condition between radiative modes propagating in the $x-z$ plane and nonradiative modes, such as SPP or waveguide modes, propagating in the $x-y$ plane is expressed as

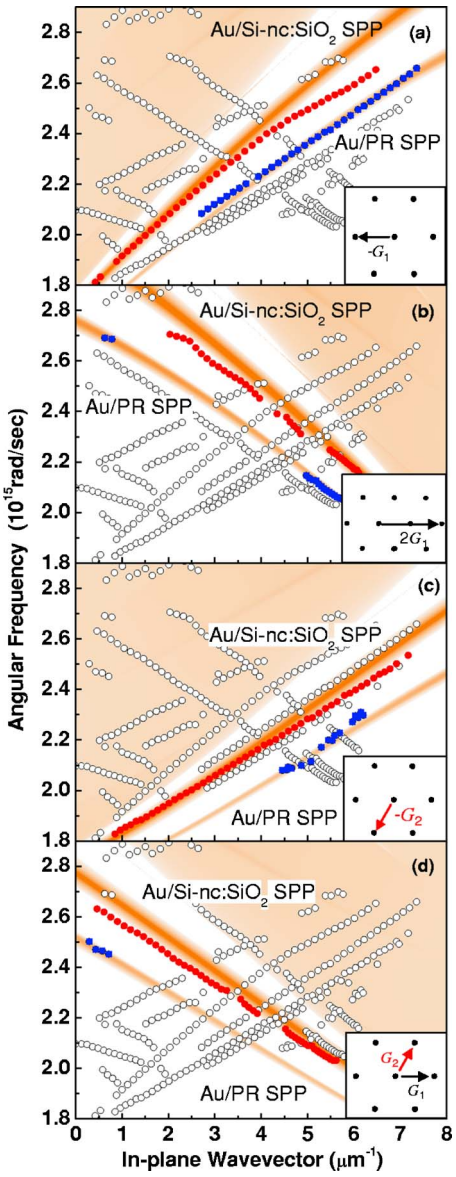

FIG. 4. (Color online) Dispersion relations for sample IIC. Circles and squares correspond to experimentally obtained data, whereas the color maps are obtained from calculation. The region deeper in color represents larger dissipated power. The scattering orders (m,n) are (a) $(-1,0)$, (b) $(2,0)$, (c) $(0,-1)$, and (d) $(1,1)$. The insets are corresponding grating vectors.

$$k_m(\omega)\begin{pmatrix}\cos\varphi\\ \sin\varphi\end{pmatrix}+mG\begin{pmatrix}1\\0\end{pmatrix}+nG\begin{pmatrix}1/2\\ \sqrt{3}/2\end{pmatrix}=\begin{pmatrix}k_{\parallel}(\omega)\\0\end{pmatrix}=\begin{pmatrix}k_0(\omega)\sin\theta\\0\end{pmatrix}, \quad (1)$$

where $k_m(\omega)$ and $k_{\parallel}(\omega)$ denote the in-plane wave vector of a guided mode and the emitted light, respectively, $k_0(\omega)$ represents the absolute value of the wave vector of the emitted light, ω is the angular frequency, φ is the azimuthal angle of the propagation of nonradiative modes, θ is the polar angle of the propagation of radiative modes, $G=|\mathbf{G}_1|=|\mathbf{G}_2|=2\pi/\Lambda$ is the grating vector with the grating period Λ, and m and n are the orders of the scattering process arising from the grating vectors $\mathbf{G}_1$ and $\mathbf{G}_2$, respectively. In order to reproduce experimentally obtained dispersion relations, we adjusted the values of the grating period and the thickness of the photoresist layer. The best result is obtained when the grating period and photoresist layer thickness are 737 and 361 nm, respectively. These values are close to measured ones. At the range of the wavelength of Si-ncs emission, SPPs experience four scattering processes, i.e., $(m,n)=(-1,0),(2,0),(0,-1),(1,1)$.

The calculated dispersion relations are shown in Figs. 4(a)–4(d) by color gradients. The insets are the corresponding grating vectors. The region deeper in color represents larger power dissipation. The strong power dissipation corresponds to the SPP modes propagating at the interface between Au and the active layer (Au/Si-nc:SiO_2 SPP), whereas the weak one to the SPP modes propagating at the interface between Au and the photoresist layer (Au/PR SPP). In Fig. 4, we can see a good agreement between the calculated dispersion relations of the SPP modes and the dispersion relations obtained experimentally. The agreement allows us to assign the origin of the observed peaks. Closed circles and squares are assigned to Au/Si-nc:SiO_2 SPP and Au/PR SPP, respectively. This analysis reveals that the four strong peaks in Fig. 3 are mediated by Au/Si-nc:SiO_2 SPP. The corresponding scattering orders are indicated in Fig. 3(d). The overall agreement implies that the strong PL peaks in Fig. 3 arise from the coupling of excitons in Si-ncs to SPPs. In Fig. 4, modes that are not identified by calculation exist. They may arise from the extraharmonic components of the grating profile.[23]

As shown in Fig. 3(c), the peaks at 740, 810, 850, and 930 nm correspond to the scattering orders $(2,0)$, $(1,1)$, $(-1,0)$, and $(0,-1)$, respectively. The intensity ratio of TM polarized emission to TE polarized one is large if the propagation direction of SPPs is close to the x direction. Therefore, the peaks at 740 and 850 nm are only TM polarized, whereas those at 810 and 930 nm have both the TM and TE polarized emission.

B. PL decay rates

The inset of Fig. 5 shows the PL decay curves for samples IIA and IIC detected at 850 nm. For sample IIC, the PL was detected from the grating side (solid curve) and the substrate side (dashed curve), whereas for sample IIA, it was detected from the substrate side (dotted curve). In order to investigate the wavelength dependence of the decay rates we measured PL decay curves in a whole emission wavelength range and estimated the decay rates by fitting the decay curves by a stretched exponential function.[24] The results are shown in Fig. 5. Closed and open circles represent PL decay rates for sample IIC detected from the grating side and from the substrate side, respectively, whereas triangles denote those obtained for sample IIA. In all cases, the decay rate increases as the emission wavelength is shortened due to the quantum size effect.[25] By placing a Au film, the decay rate is enhanced in the whole wavelength range, whereas it does not depend on whether PL comes from the grating side or the other side.

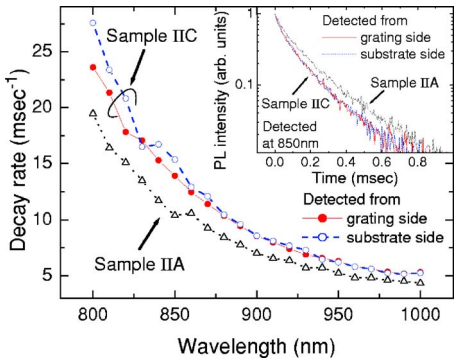

FIG. 5. (Color online) Wavelength dependence of PL decay rates for samples IIA and IIC. Closed and open circles represent PL for sample IIC detected from the grating side and from substrate side, respectively, whereas triangles denote PL obtained for sample IIA. The inset shows the decay curves detected at 850 nm. Solid and dashed lines represent PL for sample IIC detected from the grating side and from the substrate side, respectively, whereas the dotted line represents PL obtained for sample IIA.

In Fig. 6, the decay rates of sample IIC detected from the grating side normalized to those of sample IIA are plotted as a function of wavelength. We can see the increase of the normalized rate as the emission wavelength shortens. In order to analyze the wavelength dependence of the rate enhancement, we calculate power dissipation, which corresponds to the normalized decay rate, by using the same formalism to calculate the dispersion relation in the previous.[16,17] Details of the calculation procedure are found in Ref. 26. In the calculation, the contributions of dipoles positioned in the 150 nm thick active layer are averaged over the layer thickness. First, we performed calculation under the assumption that the internal quantum efficiency is 100%. However, the result did not agree with the experimental result in Fig. 6. We therefore regarded the internal quantum efficiency of Si-ncs as a fitting parameter, and the parameter was chosen so that the calculated total decay rate agreed with the experimentally obtained normalized decay rate. The best agreement was obtained when the internal quantum efficiency is 45%. The solid curve in Fig. 6 is the calculated total decay rate. We can see a good agreement between experimental and calculated results.

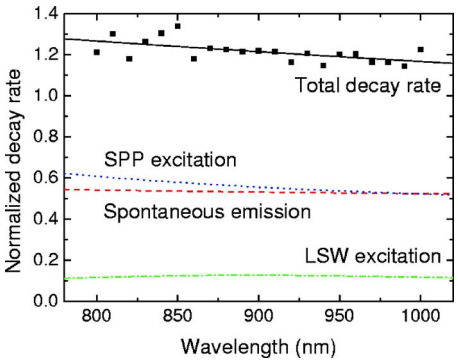

FIG. 6. (Color online) PL decay rates of sample IIC detected from the grating side normalized to those of sample IIA as a function of wavelength. Squares correspond to experimentally obtained data, whereas the solid line denote a calculated normalized decay rate. Relative contributions of radiative decay rates (dashed line), SPP excitation rates (dotted line), and LSW excitation rates (dotted-dashed line) to the total normalized decay rates are also shown.

In this calculation, we can also analyze relative contributions of different modes to which power of a dipole dissipates.[26] The contributions of the radiative decay rate, the rate of energy transfer to SPPs, and that to lossy surface waves (LSWs) to the total normalized decay rate are shown in Fig. 6 as dashed, dotted, and dotted-dashed curves, respectively. In Fig. 6, the contribution of the LSW excitation rate to the total decay rate is very small and it does not depend strongly on the wavelength. Spontaneous emission and SPP excitation rates contribute to the total power dissipation nearly equally. The spontaneous emission rate increases slightly as the wavelength shortens because of the increased photonic mode density, whereas the SPP excitation rate increases much faster. The increase of the SPP excitation rate is mainly due to larger density of state of SPPs at shorter wavelength. In Fig. 6, we can see that the wavelength dependence of the SPP excitation rate is very similar to that of experimentally obtained normalized decay rate. This means that the observed enhancement of the decay rate is mainly due to the excitation of SPPs.

Because of the energy transfer to SPPs, the recombination rate of excitons confined in Si-ncs near a Au film can be expressed as $W_{\text{total}}=W_{\text{r}}+W_{\text{nr}}+W_{\text{SPP}}$, where W_{r} and W_{nr} represent the radiative and nonradiative decay rates of Si-ncs, respectively, and W_{SPP} denotes the rate of energy transfer from excitons to SPPs. If excited SPPs are scattered with the efficiency of η_{SPP}, the PL quantum efficiency is expressed as $\eta=(W_{\text{r}}+\eta_{\text{SPP}}W_{\text{SPP}})/W_{\text{total}}$.[27] In the present work, the PL quantum efficiency is enhanced by a Au thin film and a 2D organic grating. This implies that excited SPPs are efficiently scattered by the 2D organic grating and η_{SPP} is rather large.

IV. CONCLUSION

We demonstrated that the coupling of electronic excitation of Si-ncs and SPPs supported by a Au thin film followed by scattering of the SPPs by a 2D organic grating results in strong directional PL. From the angular dependence of PL spectra, the dispersion relations were obtained and from the analysis of the dispersion relation, the excitation of SPPs was unambiguously demonstrated. The excitation of SPPs was accompanied by the enhancement of the decay rate. The wavelength dependence of the decay rate enhancement confirmed that the observed PL enhancement is due to the excitation of SPPs and efficient scattering of SPPs to photons.

Although the enhancement of PL was realized because of the coupling of electronic excitation of Si-ncs to SPPs, the enhancement was rather limited. This was because coupling between Si-ncs and SPPs and that between SPPs and photons were not optimized. In fact, the rate of SPP excitation (W_{SPP}) was not very large, i.e., comparable to the spontaneous emission rate. Further enhancement of W_{SPP} may be possible by tuning Au/Si-nc:SiO_2 SPP, which was excited more efficiently than Au/PR SPP, can be enhanced by using a metal grating instead of the combination of flat metal and an organic grating. However, although these improvements probably enhance the PL efficiency more, it is not clear whether the degree of the enhancement is enough to make Si-ncs

practical materials for light emitting devices or not. This point will be discussed after applying all possible improvements to sample structures.

ACKNOWLEDGMENT

This work is supported by a Grant-in-Aid for Scientific Research from the Ministry of Education, Culture, Sports, Science, and Technology of Japan.

[1]L. T. Canham, Appl. Phys. Lett. **57**, 1046 (1990).
[2]C. Delerue, M. Lannoo, G. Allan, and E. Martin, Thin Solid Films **255**, 27 (1995).
[3]D. Kovalev, H. Heckler, G. Polisski, and F. Koch, Phys. Status Solidi B **215**, 871 (1999).
[4]S. Takeoka, M. Fujii, and S. Hayashi, Phys. Rev. B **62**, 16820 (2000).
[5]I. Sychugov, R. Juhasz, J. Valenta, and J. Linnros, Phys. Rev. Lett. **94**, 087405 (2005).
[6]J. S. Biteen, D. Pacifici, N. S. Lewis, and H. A. Atwater, Nano Lett. **5**, 1768 (2005).
[7]J. S. Biteen, N. Lewis, H. A. Atwater, H. Mertens, and A. Polman, Appl. Phys. Lett. **88**, 131109 (2006).
[8]H. Mertens, J. S. Biteen, H. A. Atwater, and A. Polman, Nano Lett. **6**, 2622 (2006).
[9]E. Takeda, T. Nakamura, M. Fujii, S. Miura, and S. Hayashi, Appl. Phys. Lett. **89**, 101907 (2006).
[10]P. T. Worthing and W. L. Barnes, J. Mod. Opt. **49**, 1453 (2002).
[11]P. T. Worthing and W. L. Barnes, Appl. Phys. Lett. **79**, 3035 (2001).
[12]Y. Kanzawa, T. Kageyama, S. Takeoka, M. Fujii, S. Hayashi, and K. Yamamoto, Solid State Commun. **102**, 533 (1997).
[13]M. Fujii, S. Hayashi, and K. Yamamoto, in *Recent Research Development in Applied Physics*, edited by S. G. Pandalai (Transworld Research Network, Trivandrum, India, 1998), Vol. 1, p. 193.
[14]M. Fujii, A. Mimura, S. Hayashi, and K. Yamamoto, Appl. Phys. Lett. **75**, 184 (1999).
[15]J. Feng, T. Okamoto, and S. Kawata, Opt. Lett. **30**, 2302 (2005).
[16]R. R. Chance, A. Prock, and R. Silbey, Adv. Chem. Phys. **37**, 1 (1978).
[17]G. W. Ford and W. H. Weber, Phys. Rep. **113**, 195 (1984).
[18]W. L. Barnes, J. Mod. Opt. **45**, 661 (1998).
[19]D. W. Lynch and W. R. Hunter, in *Handbook of Optical Constants of Solids*, edited by E. D. Palik (Academic, Orlando, FL, 1985), Vol. 1, p. 286.
[20]D. F. Edwards, in *Handbook of Optical Constants of Solids*, edited by E. D. Palik (Academic, Orlando, FL, 1985), Vol. 1, p. 547.
[21]H. R. Philipp, in *Handbook of Optical Constants of Solids*, edited by E. D. Palik (Academic, Orlando, FL, 1985), Vol. 1, p. 749.
[22]P. A. Snow, E. K. Squire, P. St. J. Russell, and L. T. Canham, J. Appl. Phys. **86**, 1781 (1999).
[23]S. C. Kitson, W. L. Barnes, and J. R. Sambles, Opt. Commun. **122**, 147 (1996).
[24]G. Mauckner, K. Thonke, T. Baier, T. Walter, and R. Sauer, J. Appl. Phys. **75**, 4167 (1994).
[25]S. Miura, T. Nakamura, M. Fujii, M. Inui, and S. Hayashi, Phys. Rev. B **73**, 245333 (2006).
[26]T. Nakamura, M. Fujii, K. Imakita, and S. Hayashi, Phys. Rev. B **72**, 235412 (2005).
[27]K. Okamoto, I. Niki, A. Shvartser, Y. Narukawa, T. Mukai, and A. Scherer, Nat. Mater. **3**, 601 (2004).